Desalination and Water Treatment
www.deswater.com

doi: 10.5004/dwt.2017.21480

95 (2017) 262–273
November

Removal of chromium from contaminated liquid effluents using natural brushite obtained from bovine bone

José Alfredo Hernández Maldonado[a], Francisco Alejandro Torres García[a], María Mercedes Salazar Hernández[b], Rosa Hernández Soto[a,*]

[a]*Instituto Politécnico Nacional-UPIIG. Av. Mineral de Valenciana 200, Col. Fraccionamiento Industrial Puerto Interior, C.P. 36275 Silao de la Victoria, Gto, Mexico, Tel. +52 1 55 5729 6000 Ext. 81416; emails: rohernandezs@ipn.mx (R.H. Soto), jahmuam@gmail.com (J.A.H. Maldonado), fatg1991@gmail.com (F.A.T. García)*
[b]*Departamento de Ingeniería en Minas, Metalurgia y Geología, División de Ingenierías, Universidad de Guanajuato, Ex Hacienda de San Matías s/n. Fracc. San Javier, C.P. 36025, Guanajuato, Gto, Mexico, Tel. +52 473 732 22 91; email: merce@ugto.mx*

Received 29 March 2017; Accepted 22 September 2017

ABSTRACT

Natural brushite (nDCPD) obtained from bovine bone was used to remove Cr(III) from aqueous solutions. Cr(III) adsorption was performed, varying adsorbent concentration and contact time in solution. The kinetic study of Cr(III) adsorption was performed with the kinetic models of pseudo-first order and pseudo-second order, Elovich, intraparticle and external diffusions. The experimental data were examined with the Langmuir, Freundlich, Redlich–Peterson (R–P), SIPS and Temkin isothermal models. The surface of the adsorbent was characterized by various techniques. The results show that most of the kinetic adsorption data were well described by the pseudo-first-order model, the equilibrium data were best fitted to the SIPS and Langmuir models, with adsorption capacity of 43.378 and 50.767 mg/g, respectively. The equilibrium time of the system was set at 10 h. A 95% Cr(III) removal rate was achieved. The calculated thermodynamic parameters show that Cr(III) adsorption is carried out spontaneously on the surface of nDCPD, although it is positively charged, indicating that nDCPD can be a low cost and easy to obtain effective adsorbent for the removal of Cr(III) from aqueous solutions.

Keywords: Bio-adsorption; Efficiency; Kinetics; Wastewaters; Cr(III); Brushite

1. Introduction

A worldwide concern is growing, due to a considerable increase in the ecological impact of industrial effluents polluted with heavy metals such as chromium, nickel, cadmium, lead and mercury. Various industries, such as paint and pigments manufacturers, leather dyeing and tanning, fertilizers, textiles, photography, ceramics, galvanoplastics, cement and steel production and wood preservation, among others, discharge wastes without treatment into water bodies [1–7]. These industrial discharges show high concentrations of chromium dissolved, due to its high solubility in water. Chromium slowly degrades what causes it to accumulate in rivers, lakes, etc. [7–10]; water polluted with chromium is not only a constant problem for the use or reuse of it in different activities but also various diseases are generated when being consumed in an accidental manner, or by necessity in the absence of a good quality water supply system in some countries of the world [8–11]. Chromium exists in six different states of oxidation; in solution, chromium commonly occurs in the oxidation states Cr(II), Cr(III) and Cr(VI), whereas the Cr(I), Cr(IV) and Cr(V) forms are unstable; with Cr(III) and Cr(VI), the most stable forms [12,13]. Chromium in its various states of oxidation has been associated with various diseases such as allergies, respiratory problems, immune system weakening, damage to the stomach, kidneys and liver, and cancer [13–15]. The hexavalent form of chromium is more toxic than the trivalent form, because it is highly soluble and moves

* Corresponding author.

easily through the soil, it is also a powerful oxidizing agent that can be absorbed through the skin [14]. On the other hand, Cr(III) in trace concentration is necessary for glucose metabolism in human nutrition, as well as for plants and animals [12]; however, prolonged exposure to Cr(III) can cause cancer, and even under certain conditions it can oxidize and damage the surrounding flora and fauna [12–14]. Comparatively, Cr(VI) is about 100 times more toxic and 1,000 times more mutagenic than Cr(III), so the maximum established concentration of these compounds in wastewaters has been set at 5 mg/L for Cr(III) and 0.05 mg/L for Cr(VI) [14–16]. The environmental impact generated by these compounds has prompted the scientific community to develop different methods to treat industrial effluents containing these substances. Some are precipitation, oxide-reduction, ion exchange, filtration, electrochemical treatment, membrane technologies and evaporation recovery; however, some of these methods are costly and inefficient, especially when the metal concentration is low [6–19]. Additionally, the formation, disposal and storage of sludge and wastes, which originate during the processes of removal, become a major problem to solve [14–16]. In addition, the elimination of these pollutants has been studied by means of adsorption, a method considered economical and efficient, due inter alia to the diversity of low-cost adsorbents and their possible reuse [6–22]. Bio-adsorption of metal ions from wastewaters is one of the most promising technologies, due not only to the low cost of bio-adsorbents but also to the considerable decrease in the volume of chemical sludge that must be removed by the method; bio-adsorption also stands out for its high efficiency of heavy metals removal even in highly diluted effluents [15–19]. In recent years, research on low-cost bio-adsorbents for the removal of heavy metals has been intensified, highlighting various agricultural residues and industrial byproducts [1,8,22–24]. Among the materials that have been studied in the removal of chromium from wastewaters, are rice bran [2,3], wheat bran [5,6], *Enteromorpha* sp. [7], orange peel pith [9,10,], *Strychnos nux-vomica* shell [11], *Caryota urens* biomass [12], *Swietenia mahagoni* shell [13,15], *Colocasia esculenta* leaves [16], algal biomass [14,19], tamarind seeds [18] and lignocellulosic residues [20], among others. In addition, natural polymers have been used; among these materials we can find apatites, mineral compounds relatively common in nature, and the main source of phosphorus and phosphate in the engineering of bone tissues, given their bio-activity and biocompatibility [25–31]. These are also used as support in various catalytic reactions and help remove toxic elements from soils and wastewaters [32–39]. Hydroxyapatite stands out because it shows chemical and structural similarities to the main mineral phase constituent of bones and teeth in vertebrates. It has also been used in bio-adsorption processes of various metals, showing good results when compared with other bio-adsorbents. Its use in the removal of chromium ions from aqueous solutions has reached percentages greater than 90% [1,8,29,40–42]. Brushite ($CaHPO_4{\cdot}2H_2O$) – another compound of the apatite family, commonly used as bone cement [43] – has been used in dye, Cu, Pd, malathion and the removal of fluoride ions [44–48]. In most studies, it also shows higher percentages in the removal of contaminants when compared with those obtained from hydroxyapatite [45,48]; however, the ability to remove Cr(III) with brushite has not been analyzed; consequently, the objective of the present work is to analyze the adsorption process of Cr(III) ions in natural brushite obtained from bovine bone (nDCPD) and, once established this mechanism, determine the adsorbent/solution ratio effect used in the adsorption, in order to compare the obtained Cr(III) removal efficiency with values reported for hydroxyapatite.

2. Methods and materials

2.1. Materials

All reagents used were analytical grade. Deionized water was used to prepare test solutions at 0 to 0.03 mM concentrations. Chromium salt (2Cr (OH) SO_4 x Na_2SO_4) was donated by the company Cuero Centro, S.A. de C.V., Mexico.

2.2. Preparation of adsorbent

Natural brushite (nDCPD) was obtained from bovine bone, and then washed with hot water, until the elimination of adhered residues. Immediately after bones were dried in a convection oven (Shel Lab, Cornelius, OR, model CE5F) at 353 K for 24 h, they were then crushed with a ball mill and screened to obtain a particle size of 104 μm (150 mesh). 1 g of the obtained powder was treated at room temperature with 50 mL of solution of HCl 10^{-2} M with vigorous stirring for 30 min, then the solution was decanted and immediately, thereafter, the powder was mixed with 50 mL of NaOH, 10^{-2} M solution, maintaining vigorous stir at room temperature for 30 min. Subsequently, the powder was filtered and dried in a convection oven at 353 K for 24 h [49].

2.3. Analysis of nDCPD through thermogravimetry

The thermogravimetric analysis (TGA) of nDCPD was performed in a scale (STA 409 EP NETZSCH) placing 20 mg of sample in an aluminum basket. The sample was heated starting at room temperature reaching 700°C with a heating rate of 10°C/min [50].

2.4. Determination of the isoelectric point

The determination of the natural brushite isoelectric point was performed by mass titration method, using a Thermo Scientific (Orion 4 Star) pH meter, where 20 mg of the sample are suspended in water at room temperature, 24 h later, time at which pH reaches equilibrium, the pH of the suspension around the solid was measured. After that, other 20 mg of the sample were added to the suspension and it was kept at rest for 24 h so that the suspension reaches equilibrium. The whole process was repeated until the pH of the suspension remained constant regardless the amount of added solids, this pH value being the point of zero charge of brushite [51].

2.5. Characterization of nDCPD

X-ray diffraction (XRD) patterns were obtained on a diffractometer (Ultima IV, Rigaku, Japan). The Fourier transform infrared sample studies were performed with a Spectrum 100 Analyzer (PerkinElmer, United States) in KBr

pellets, measuring in a range of 400–4,000 cm^{-1}, 32 scans were obtained with a resolution of 4 cm^{-1}. Scanning electron microscopy (SEM-EDS-EDX) images were obtained in a JOEL (6510 plus). The X-ray energy dispersion spectroscopy (EDS) analysis was performed with a spectrometer. The adsorption spectra in the UV-Vis region were obtained with a spectrophotometer and the chromium content in nDCPD was determined using atomic absorption equipment (AAnalyst-100, PerkinElmer).

2.6. Cr(III) adsorption isotherm

Different isotherm models are proposed in the literature that describes the adsorption of Cr(III) in the obtained brushite. Models and equations used are displayed in Table 1 [52,53]. The regression coefficient was calculated to evaluate the fit of each nonlinear model and the separation factor, R_L, which predicts the affinity between adsorbent and adsorbate. Represented by the following equation [53]:

$$R_L = \frac{1}{1 + K_L C_0} \tag{1}$$

where K_L is the Langmuir model constant (L/mg) and C_0 is the initial Cr(III) concentration (mg/L). With the help of Eq. (2), the adsorption process spontaneity was determined by calculating the change in the apparent Gibbs free energy: ΔG (kJ/mol) at 25°C [54]:

$$\Delta G = -RT \ln\left(55.5 K_L\right) \tag{2}$$

where K_L is the Langmuir model constant (L/mol), R is the ideal gases constant (kJ/mol K) and T is the absolute temperature (K). In order to generate the Cr(III) adsorption isotherms in nDCPD we put in contact 1 g of sorbent with 50 mL of Cr(III) solution, varying the concentration of the solution between 0 and 0.03 M. The mixture was held in a shaker (ZHWY-200D) with a 200 rpm at 25°C and a 24 h contact time.

Table 1
Models of non-linear adsorption isotherm

Model	Equation
SIPS	$q_e = \frac{q_m (K_s C_e)^{n_s}}{1 + (K_s C_e)^{n_s}}$
Redlich–Peterson (R–P)	$q_e = \frac{K_R C_e}{1 + a_R C_e^{\beta}}$
Langmuir	$q_e = \frac{q_m K_L C_e}{1 + K_L C_e}$
Temkin	$q_e = A + B \ln(C_e)$
Freundlich	$q_e = K_F C_e^{1/n}$

q_e, concentration of Cr(III) in equilibrium with the solid phase (mg/g); C_e, Cr(III) concentration in the liquid phase (mg/L); q_m, maximum Cr(III) concentration adsorbed by the adsorbent mass; K_S, SIPS constant related to energy adsorption; n_S, SIPS model dimensionless parameter; β, exponent (0 < β < 1); K_R and a_R, R–P constants; K_L, Langmuir model constant related to the energy adsorption of the adsorbent; A and B, Temkin model constants; K_F, Freundlich model constant related to the adsorption capacity and 1/n, adsorption reaction energy.

2.7. Cr(III) adsorption kinetics

Kinetic experiments on nDCPD of Cr(III) bio-adsorption were carried out in batches. The first assay was performed varying the concentration of nDCPD (C_{ads}), from 0 to 40 g/L in the solution, maintaining the contact for 24 h at 200 rpm and 25°C. Samples were taken every 90 min, and centrifuged in a Hermle Z-383 K at 10,000 rpm for 10 min. The absorbance of each supernatant was determined with a UV-Vis spectrophotometer (Jenway 6705), and the Cr(III) concentration present in the solution was determined using a UV-Vis spectrophotometer (Jenway 6705). The amount of Cr(III) adsorbed in nDCPD, q_e, was obtained using the following equation [4]:

$$q_e = \frac{V\left(C_0 - C_e\right)}{m} \tag{3}$$

where C_0 is the initial concentration and C_e is the Cr(III) concentration through time t (also named concentration of equilibrium) expressed in mg/L. V is the solution volume (L) and m is the mass of nDCPD (g). The Cr(III) removal percentage, % R_{Cr}, was calculated using the following equation [5]:

$$\%R_{Cr} = \frac{\left(C_0 - C_e\right)}{C_0} \times 100 \tag{4}$$

Besides using a determination coefficient to compare the efficiency of different kinetic models, the normalized standard deviation, Δq, was calculated with the following equation [54]:

$$\Delta q = 100 \times \sqrt{\frac{\left(\frac{q_{exp} - q_{cal}}{q_{exp}}\right)^2}{N - 1}} \tag{5}$$

where N is the number of data, and q_{exp} and q_{cal} (mg/g) are, respectively, the experimental and calculated values of Cr(III) ions adsorbed in equilibrium.

2.8. Experimental data of Cr(III) removal

The reversibility of Cr(III) adsorption in nDCPD was assessed with equilibrium Cr(III) removal experiments. The kinetic experiment described in section 2.7 produced nDCPD loaded with Cr(III), which was put in contact with a 40 mL 0.5 M NaOH solution for 24 h. The amount of Cr(III), which remained adsorbed on nDCPD, was calculated by mass balance using Eq. (6) [8]:

$$q_d = q_0 - \frac{V}{m} C \tag{6}$$

where q_0 is the amount of Cr(III) initially adsorbed (mg/g). q_d is the amount of chromium that remained adsorbed in nDCPD (mg/g), C is the Cr(III) concentration in the solution (mg/L), V is the NaOH solution volume (L) and m is nDCPD mass (g).

The percentage of Cr(III) removal was determined by Eq. (7):

$$\%\ \text{Des} = \frac{(q_0 - q_d)}{q_0} \times 100 \tag{7}$$

where % Des is the percentage of Cr(III) removed from the adsorbant, q_o is the amount of Cr(III) adsorbed by the adsorbant and q_d is the amount of Cr(III) removed from the solution.

3. Results and discussion

3.1. The contact time effect and the amount of adsorbent

The adsorption process of Cr(III) in nDCPD has different moments (Fig. 1(a)). In the first period, from 0 to 10 h, a high rate of chromium adsorption is displayed; while the second stage, this is, after 10 h of contact, is characterized by a slow adsorption period, most likely because the active fixation sites of Cr(III) over nDCPD were occupied during the first stage. Finally, after 20 h of contact, the chromium adsorption in nDCPD reaches its equilibrium due to the saturation of active sites with Cr(III). These results are consistent when egg shell dust is used as an adsorbent [55]. Regarding the removal of Cr(III) (Fig. 1(b)), which also shows three moments with the same time intervals obtained in the adsorption experiment, Fig. 2 shows that the amount of Cr(III) removal depends directly on the adsorbent concentration in the solution, suggesting that all available sites for chromium capture are rapidly saturated due to the large amount of this element present in the effluent. A similar behavior has been reported when using synthetic brushite to remove Cu and Pd ions [48], with removal percentages between 70% and 90%. In the present work, a 95% percentage of removal of Cr(III) from aqueous solutions was achieved, suggesting that nDCPD has anion removal capacity similar to synthetic brushite. This behavior was also observed when using *Ruellia patula* Jacq as Cr(VI) bio-adsorbent [56]. Although in some cases it has been reported that increasing the adsorbent concentration decreases Cr(VI) adsorption capacity [11,15,57,58], this effect is attributed to the obstruction of the active sites in the adsorbent.

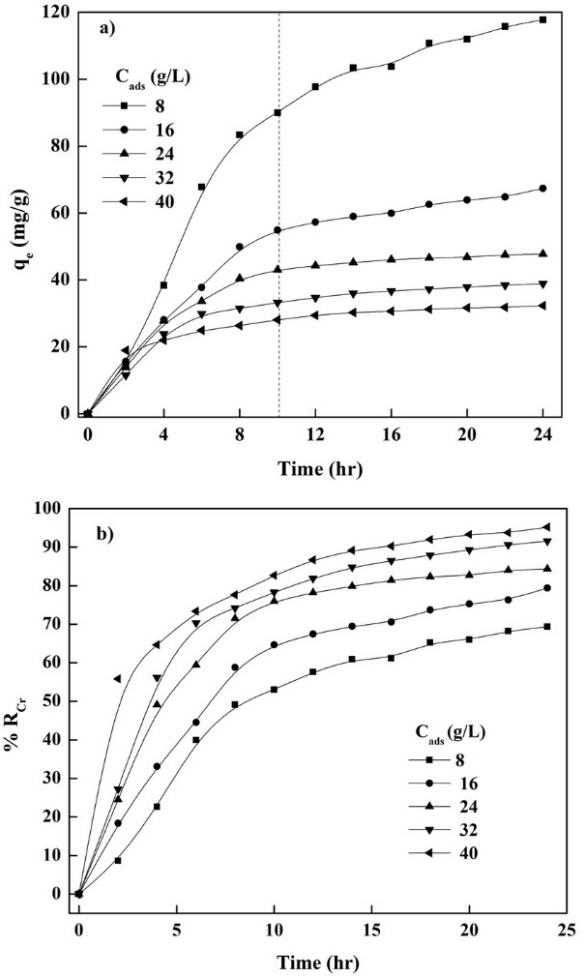

Fig. 1. Effect of contact time on Cr(III) (a) adsorption and (b) removal.

3.2. Analysis of nDCPD using thermogravimetry

Brushite is stable under 100°C and after the process of mass loss that the sample experiences from 150°C, the mass of the sample is again stabilized at 300°C (Fig. 3). Therefore, considering that Cr(III) adsorption experiments in the present study were carried out at room temperature, it was not necessary to perform a complete TGA.

3.3. Estimation of the point of zero charge

The zero charge value of nDCPD was 6.3, a value similar to 6.2 for brushite obtained by chemical synthesis [45]. The Cr(III) solution used in the present study had an initial pH of 2.1. At these pH values the surface of nDCPD is positively charged causing Cr(III) ion adsorption to be disadvantaged due to electrostatic repulsion between Cr ions and the surface of nDCPD; however some authors consider that the adsorption of Cr ions on the surface of the positively charged adsorbent is carried out as a consequence of the ion exchange process between species [8,48]. In the case of nDCPD, the species that can act in this exchange process are Ca(II) present on the surface of the adsorbent and Cr(III) present in the solution. In order to confirm

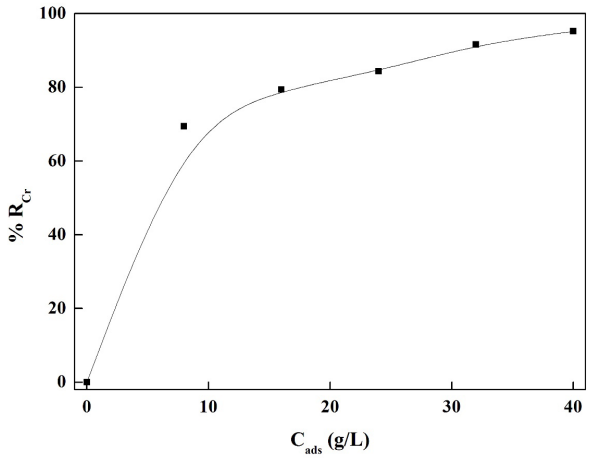

Fig. 2. Effect of adsorbent concentration on Cr(III) adsorption.

some of the two exchange mechanisms, FTIR and energy dispersive X-ray analysis (EDXA) studies were performed in order to know the changes that the nDCPD structure undergoes after being in contact with Cr(III) solutions.

3.4. Adsorption isotherms

The equilibrium data analyzed with adsorption isotherms allows us to understand the interaction between Cr(III) and nDCPD, providing a model that describes the adsorption behavior in the solution. Models used for the adsorption mechanism analysis are concentrated in Table 1. Fig. 4 shows the adsorption isotherms obtained by each of the applied models. Parameters obtained in each model along with the determination coefficient (R^2) are shown in Table 2. We determined that the Langmuir and SIPS models are the most appropriate to describe the Cr(III) adsorption process in nDCPD, since obtaining a value of $\beta = 1$ in the R–P model makes its equation transform to the Langmuir isotherm. This transformation is due to the nature of the R–P model, which originates from the combination of Freundlich and Langmuir isotherms, as well as the SIP model. The obtained data show an adsorption process forming a monolayer occurring on the sorbent surface, which is confirmed in the Freundlich model by an n value higher than one, thus revealing that the adsorption process is physical. On the other hand, the obtained Gibbs free energy value was negative (–23.87 kJ/mol), indicating a spontaneous adsorption process [53] and a strong interaction between Cr(III) ions and the nDCPD surface, as pointed out in studies of dye adsorption with agroindustrial residues [54]. Separation factor values obtained between 0 and 1 show a favorable Cr(III) adsorption in nDCPD, and it should be noted that this trend can be seen independently of the equilibrium model.

When comparing the Cr(III) adsorption capacity of several natural adsorbents [19,56] such as synthetic hydroxyapatite [8] and brushite in adsorption equilibrium studies of Cu, Pb and F [45,47–48], we observed that all adsorption data obtained in the current work bear resemblance with similar studies [59]. Therefore, we consider nDCPD as an appropriate material to remove Cr(III) from aqueous effluents.

3.5. Kinetic studies

The analysis of different Cr(III) adsorption kinetics models in nDCPD (Table 3) is useful to recognize the process

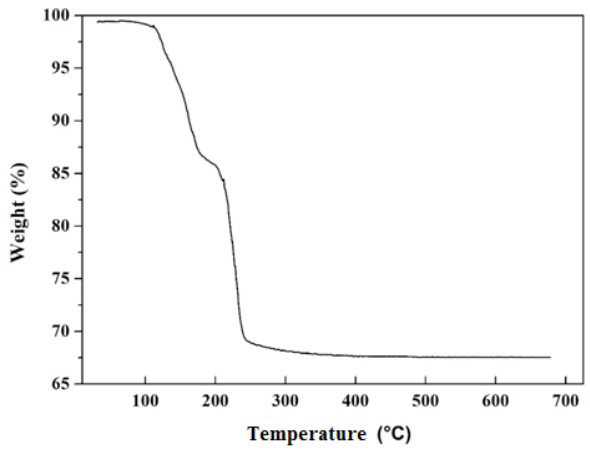

Fig. 3. Analysis of nDCPD through thermogravimetric analysis (TGA).

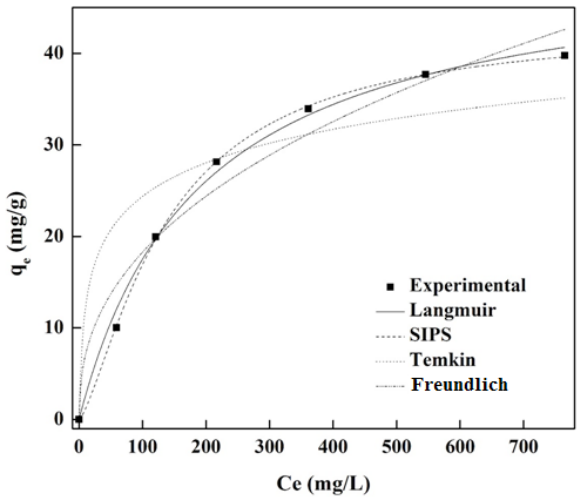

Fig. 4. Different isothermal adsorption models of Cr(III) with nDCPD.

Table 2
Different adsorption models parameters for Cr(III) adsorption by batch

Models	Parameters			
SIPS	K_S (L/mg)	q_m (mg/g)	n_S	R^2
	0.011	43.378	1.379	0.9998
Redlich–Peterson	K_R (L/g)	a_R (L/mg)$^\beta$	β	R^2
	0.2673	0.0053	1.0	0.9986
Langmuir	K_L (L/mg)	q_m (mg/g)	R_L (L/mg)	R^2
	0.0053	50.767	0.026–0.26	0.9950
Freundlich	K_F (mg/g)(L/mg)$^{1/n}$	n		R^2
	2.6882	2.4024		0.9651
Temkin	A (L/mg)	B (kJ/mol)		R^2
	1.74×10^{-8}	5.293		0.8425

Table 3
Adsorption isotherm models used for the experimental data analysis

Model	Equation	Reference
Pseudo-first order	$\frac{dq}{dt} = K_1(q_e - q)$	[46]
Pseudo-second order	$\frac{dq}{dt} = K_2(q_e - q)^2$	
Elovich	$\frac{dq}{dt} = \alpha e^{-\beta q}$	
Intraparticle diffusion (DI)	$q = k_{id} t^{0.5}$	
External diffusion (DE)	$\ln\left(\frac{C}{C_0}\right) = -k_{ext} t$	[47]

controlling adsorption, which can be a mass transfer or a chemical reaction. Models applied to experimental data (Fig. 5) show the pseudo-first-order model as the one that best fits the data; except for the kinetics performed with the maximum adsorbent concentration (Fig. 5(e)) which was fitted appropriately with pseudo-second-order model, taking as the first criterion the value of the determination coefficient, which in all cases was greater than 0.99 [6]. The standard deviation normalized for each model (Table 4) confirmed our observations with the determination coefficient, whilst in the case of kinetics, adjusted with two different models, the Δq value points out the pseudo-second-order model as the best fit.

To understand the mass transfer mechanism in the adsorption process, which can be limited by external or intraparticle mass transfer, and since the transport of the sine of the solution and adsorption are seldom the process restriction steps, it is necessary to analyze Fig. 1(a), which evidently shows two stages. The first stage can be attributed to a near-instantaneous capture of Cr(III), due to the availability of binding sites on the nDCPD surface. In the second stage, we infer that the system equilibrium has been reached, given the decreasing tendency of the isotherm slope. To find the limiting phenomenon in the adsorption process, we determined the rate of constants of each step and listed them in Table 5. Data show a $k_1 > k_2$ constants order, indicating a high rate of adsorption at this stage. In contrast, the second stage evidences a mass transfer resistance due to the decrease of chromium ions diffusion within pores of the adsorbent, causing a considerable reduction in the adsorption rate of chromium, until equilibrium is reached. These results exhibit the external diffusion model as the least appropriate to adjust the Cr(III) adsorption kinetics, which is consistent with similar studies [59].

3.6. Cr(III) removal study

Results obtained in the removal process (Fig. 6) suggest a Cr(III) removal rate on the surface of nDCPD dependant of the desorbent concentration. This indicates that a portion of ions bound on the surface of the adsorbent are easily removed due to their low adsorption energy, consequently increasing the number of available sites for ions as the adsorbent concentration increases. Similar results are obtained using wheat bran as an adsorbent [5], although in that case, chromium was completely removed as pH was increased. On the other hand, the maximum amount of Cr(III) removal achieved was 26% in 24 h, indicating that much of the chromium was chemosorbed in nDCPD, concurring with studies using carbonized bone [8]. Similar results were reported with the processes of Cr(VI) removal [7,60], using the same concentration of NaOH solution, suggesting that the process of removal of Cr(III) on the surface of brushite, depends directly on the NaOH concentration used [57].

3.7. Characterization of nDCPD

The XRD pattern of nDCPD, shown in Fig. 7, is in agreement with results reported for brushite in the database of JCPDS-International Center for Diffraction Data Cards [61]. In contrast, the sample doped with Cr shows that peaks at 32°, 33.4° and 40° decrease in intensity, relating to the presence of Cr ions in apatite. On the other hand, peaks appearing at 26.5°, 34.3° and 39.7° can be assigned to the Cr ions with the help of $CrCl_3$ as a comparison pattern (Fig. 8), this causes a decrease in the network parameter from 5.77 [62] to 3.85 and an average crystal size (from 9.26 to 5.12 Å), this decrease is due to the substitution of Ca(II) by Cr(III), which have a radius of 1.12 [63] and 0.66 Å [64], respectively, confirming the presence of Cr(III) within the structure of nDCPD.

The infrared spectrum of nDCPD (Fig. 9) shows two doublets at 3,548; 3,484 cm^{-1} and 3,278; 3,166 cm^{-1}, attributed to the OH stretching of the water molecule in brushite. The peak at 2,944 is due to the stretching of PO–H occurring in HPO_4^{-2} [65]. At 2,385 cm^{-1}, a peak is attributed to a combination of bands or a harmonic. A shoulder observed at 1,725 cm^{-1} is related to the flexural stress of the water molecule [66], while the vibrations at 1,651 and 665 cm^{-1} are related, respectively, to physical and vibrational water link modes. The vibration at 1,215 cm^{-1} is due to the flexion of the O–H plane and at 790 cm^{-1} it is due to P–O–H flexion outside the plane. Peaks at 1,138; 1,120; 1,065 and 1,004 cm^{-1} are attributed to the P–O stretch, whereas 987 and 873 cm^{-1} peaks are related to the P–O (H) stretch in the HPO_4^{-2}. The bending vibrations of phosphate groups within brushite are observed in the doublet at 577, 526 cm^{-1} [65]. In the nDCPD–Cr spectrum, several vibrations disappear and/or decrease their intensity in regards to nDCPD. Among them are the vibrations assigned to the OH– and PO_4^{3-} groups, which confirms that the Cr(III) adsorption mechanism is carried out by the substitution of Ca(II) ions in the phosphate species present on the surface of nDCPD, this type of phenomena was reported for carbonized bone [8], which shows that since it belongs to the apatites family, nDCPD can adsorb Cr(III) even though the surface is positively charged.

Fig. 10 shows the adsorption spectra in the UV-Vis region of pure nDCPD and Cr-doped. In non-doped nDCPD, two bands appear at 290 and 385 nm, and are significantly affected by the presence of Cr. The first band disappears in the nDCPD–Cr spectrum, while the second band is covered by a strong adsorption band at 435 nm, and an additional band is visible at 585 nm. Both peaks are related to the presence of Cr(III) in nDCPD, which is consistent with our IR spectra observations, where some bands are absent in the Cr-doped nDCPD sample, in contrast to the pure nDCPD sample. The IR spectrum shows a shoulder at 680 nm in the

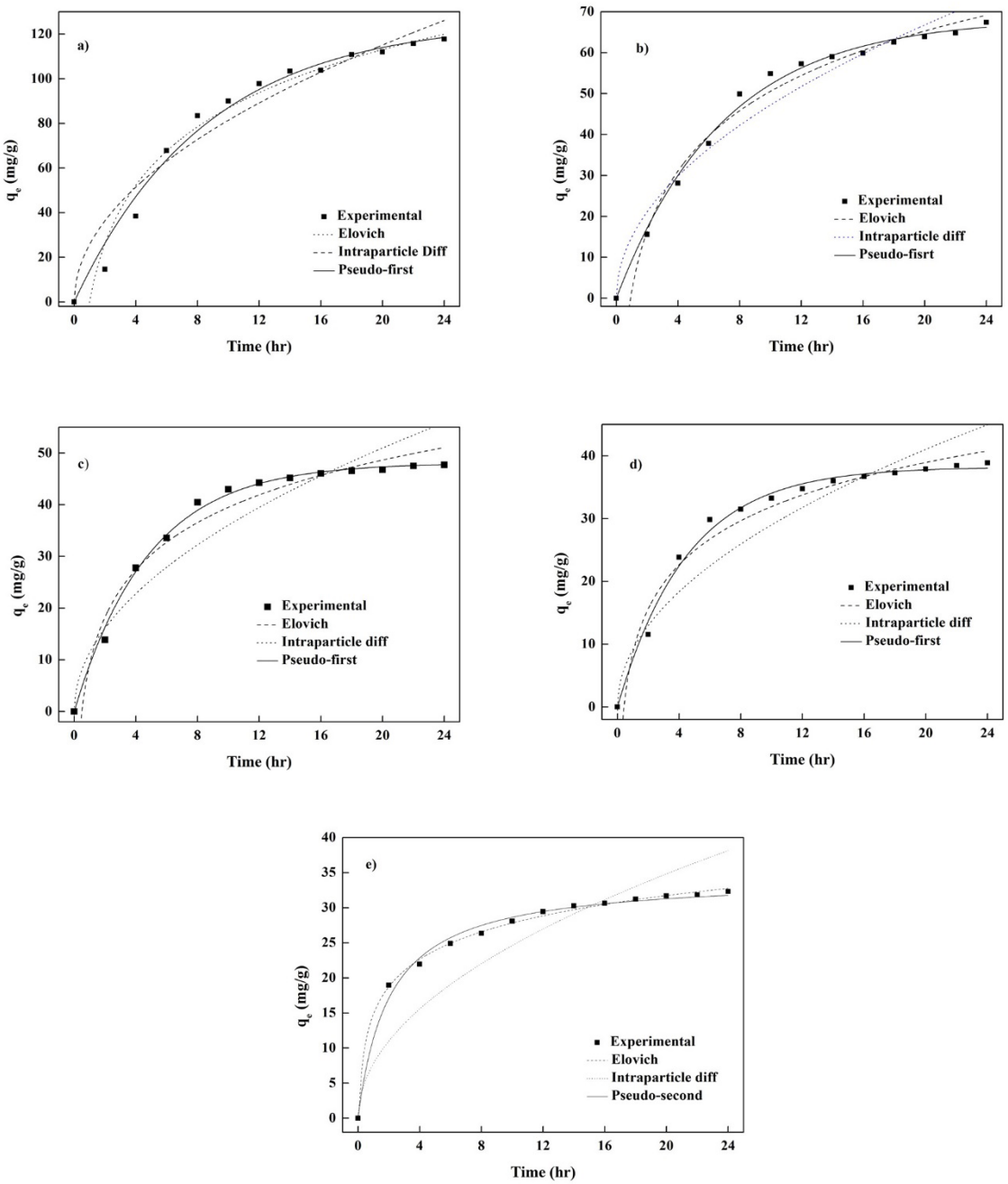

Fig. 5. Adjustment of different kinetic models at different adsorption concentrations: (a) 8, (b) 16, (c) 24, (d) 32 and (e) 40 g ads/L.

Table 4
Best fit kinetic parameters for Cr(III) bio-adsorption in nDCPD

C_{ads} (g/L)	Pseudo-first order				Pseudo-second order			Intraparticle			
	q_{exp} (mg/g)	q_e (mg/g)	K_1 (h^{-1})	R^2	q_{cal} (mg/g)	K_2 (mg/g h)	R^2	q_{cal} (mg/g)	k_{id} (mg/g $h^{0.5}$)	R^2	Δq_e, %
8	90.941	126.005	0.117	0.990	174.126	0.0006	0.975	136.339	0.2367	0.9421	8.033
16	50.314	68.338	0.144	0.993	89.391	0.0015	0.988	177.120	0.3075	0.9511	7.614
24	39.592	48.067	0.207	0.996	58.588	0.0038	0.984	232.185	0.4031	0.8764	5.108
32	35.628	38.214	0.221	0.992	46.070	0.0056	0.998	283.737	0.4926	0.8691	0.358
40	38.688	34.429	0.337	0.965	34.429	0.0143	0.992	337.881	0.5866	0.7368	1.005

Table 5
Parameters of adsorption rate for the different stages

C_{ads}, g/L	k_1, mg/g min$^{0.5}$	k_2, mg/g min$^{0.5}$
8	50.0699	15.4114
16	23.1666	6.8512
24	18.4146	2.6712
32	17.8350	3.4710
40	4.9458	1.7674

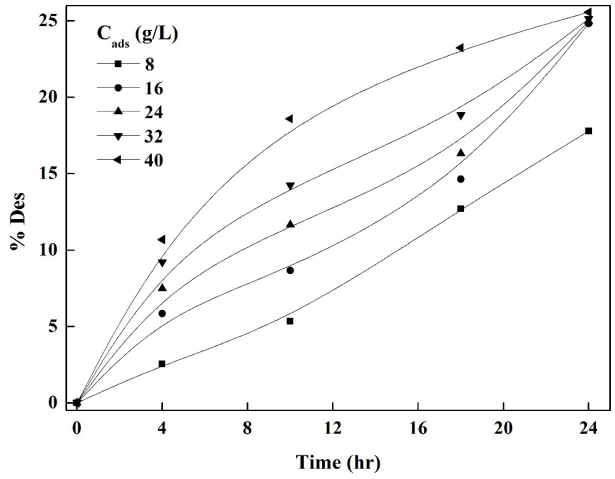

Fig. 6. Evolution of Cr(III) removal at different concentrations of adsorbent with a solution of 1 M NaOH.

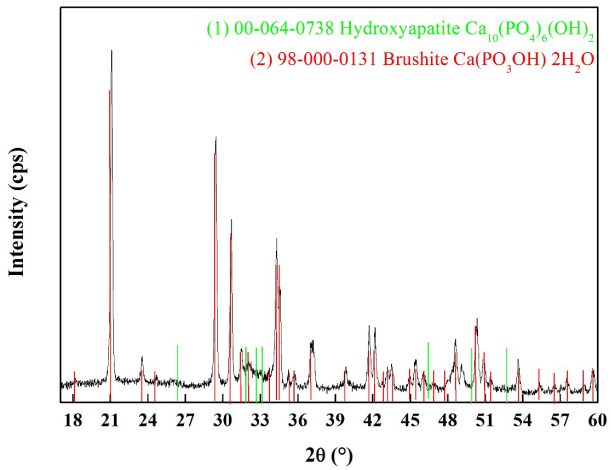

Fig. 7. X-ray diffraction pattern of nDCPD compared with two apatites: (1) hydroxyapatite and (2) brushite.

Cr-doped sample, which could reveal the presence of Cr(III) in pseudo-tetrahedral form [67].

The SEM image of nDCPD (Fig. 11(a)) shows well-defined monoclinic dish morphology, characteristic of brushite [68]. Chromium clusters are also found on the surface of the nDCPD morphology (Figs. 11(b) and (c)). The composition of samples was analyzed by EDS, showing

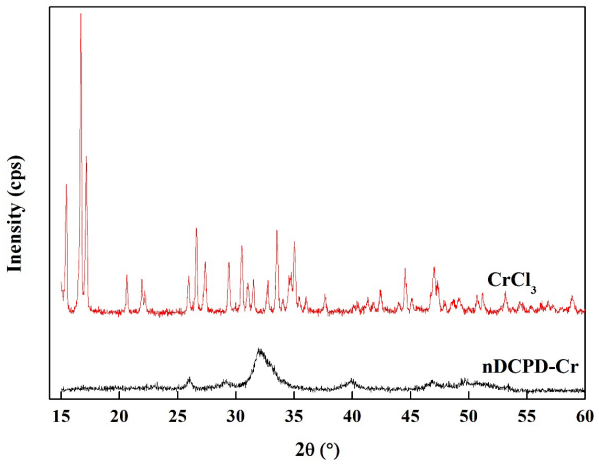

Fig. 8. X-ray diffractograms of nDCPD–Cr and $CrCl_3$ standard.

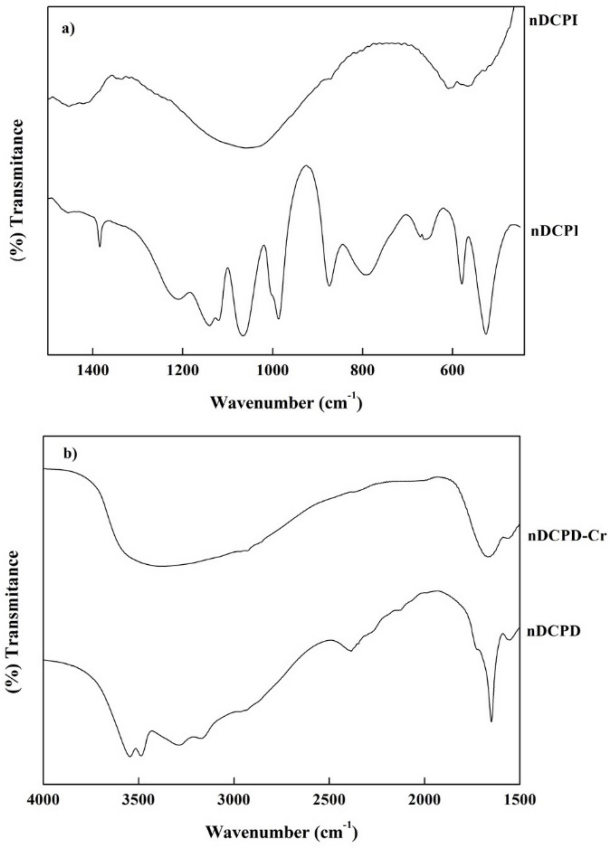

Fig. 9. Infrared spectra of nDCPD and nDCPD–Cr, (a) 1,500 to 450 cm^{-1} and (b) 4,000 to 1,500 cm^{-1}.

an almost stoichiometric Ca/P ratio in nDCPD, thus confirming the incorporation of Cr in the sample. While the increase in the Ca/P ratio in nDCPD is due to the presence of Cr causing a decrease of phosphate groups on its surface, as evidenced by the elemental analysis of nDCPD and nDCPD–Cr shown in Table 6. The elemental mapping of the sample confirms the homogeneous incorporation of Cr into nDCPD (Figs. 11(d) and 12) confirming the hypothesis

that all bands found in UV-Vis are caused by the presence of Cr(III) ions, along with the loss of vibrations of HPO_4^{-2} groups, causing significant changes to the apatite surface structure, determined by XRD through the particle size and network parameter.

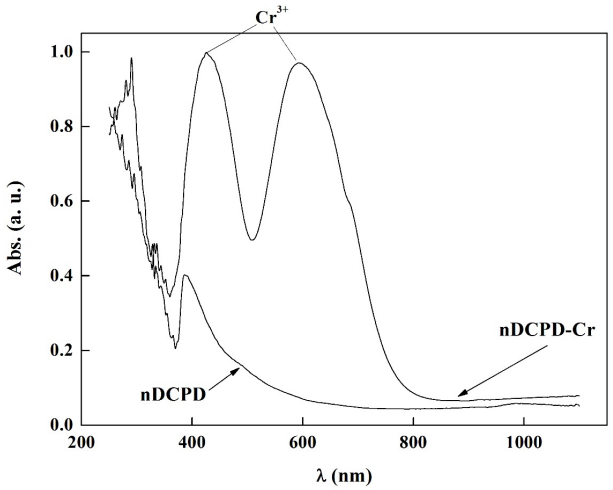

Fig. 10. Adsorption spectra in the UV-Vis region of pure and Cr-doped nDCPD.

4. Conclusion

The results obtained show that natural brushite obtained from bovine bone (nDCPD) has a high capacity to remove chromium from aqueous solutions at room temperature. The calculated thermodynamic parameters indicate that the adsorption capacity of nDCPD is comparable with the synthetic brushite adsorption capacity. The percentage of Cr(III) removal achieved was greater than 95% without the need to control the pH of the medium. The studies of adsorption of Cr(III) in equilibrium show that the isothermal adsorption models SIPS and Langmuir are the most appropriate for this system, and also reveal that the biosorption process is carried out spontaneously on the surface of nDCPD, which was confirmed by XRD, FTIR analysis and SEM images of nDCPD samples, which exhibited significant surface changes.

Table 6
Elemental analysis of nDCPD and nDCPD–Cr samples

Element	nDCPD	nDCPD–Cr
C	55.78	55.08
O	35.9	28.03
P	3.89	2.12
Ca	4.43	1.25
Cr	0	13.52

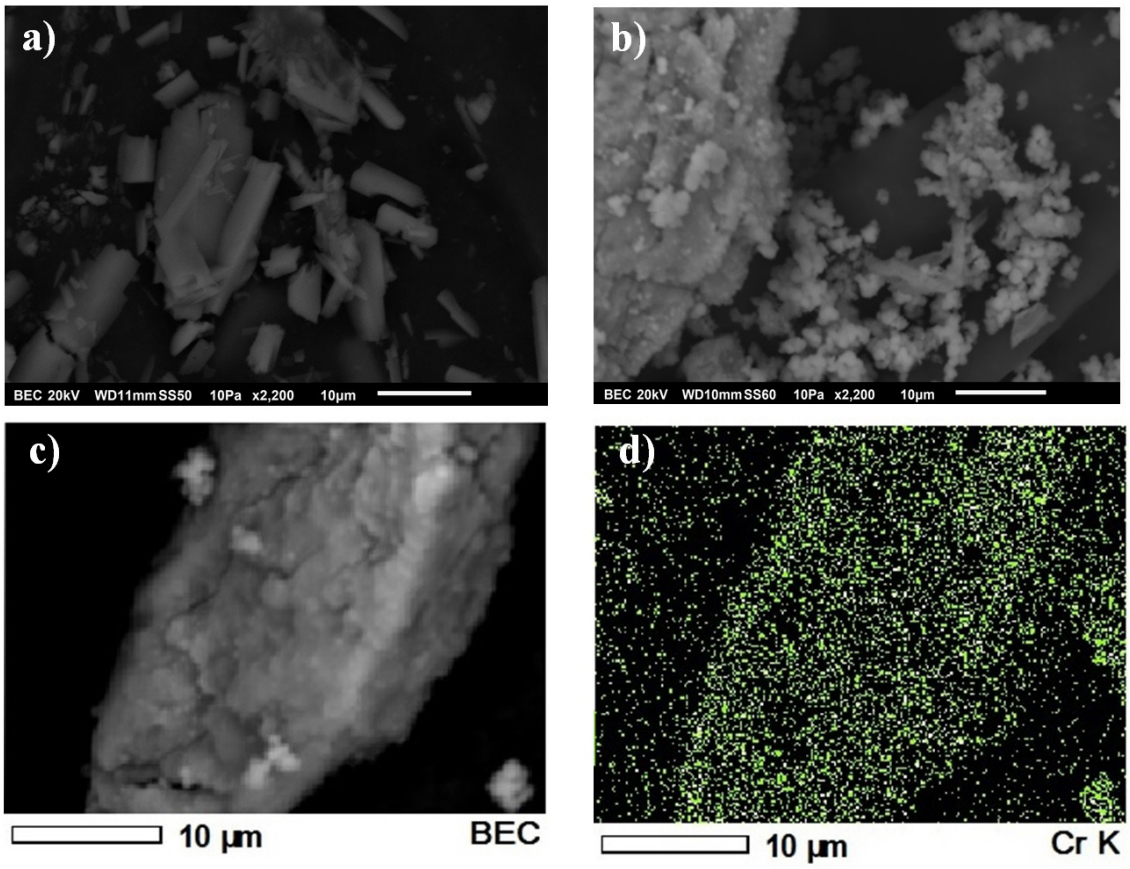

Fig. 11. Images obtained in SEM. (a) nDCPD, (b) and (c) nDCPD–Cr, (d) chromium mapping analysis in nDCPD.

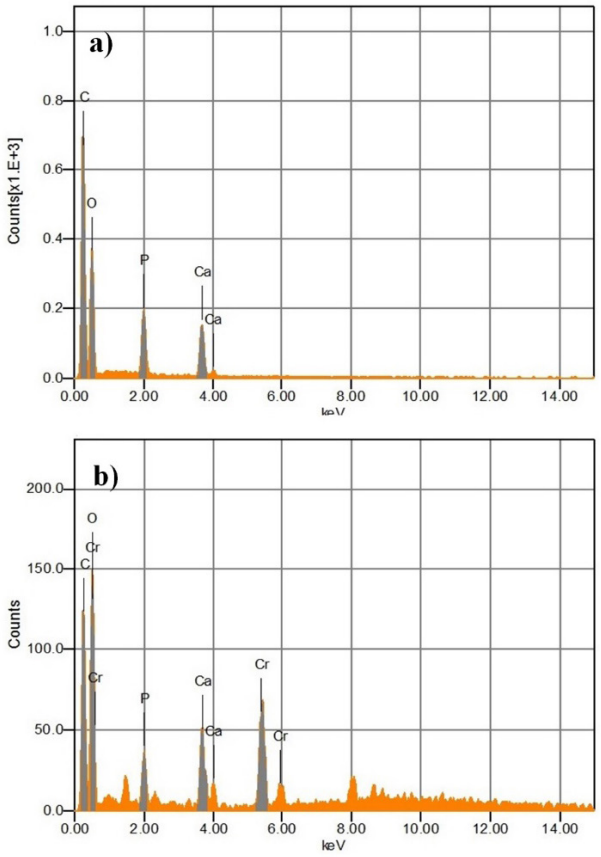

Fig. 12. EDXA elemental and spectral mapping of (a) nDCPD and (b) nDCPD–Cr.

The adsorption kinetics of Cr(III) in nDCPD demonstrate that the process is carried out in three stages. The pseudo-first-order model appropriately describes the experimental data obtained, indicating that the phenomenon that dominates the overall transfer process is the number of adsorption-free sites. Given the above, it is possible to conclude that nDCPD, a low cost and easy to obtain material, can be effectively used in the removal of Cr(III) from contaminated effluents, without the need to control process variables such as pH and temperature, significantly influencing the final cost of the removal process.

Symbols

A	—	Temkin isotherm equilibrium binding constant, L/mg
a_R	—	Redlich–Peterson model constant, L/mg
B	—	Temkin isotherm constant, kJ/mol
C_0	—	Cr(III) initial concentration, mg/L
C_e	—	Cr(III) concentration in the liquid phase, mg/L
K_F	—	Freundlich model constant related to the adsorption capacity, $(mg/g)(L/mg)^{1/n}$
K_L	—	Langmuir model constant, mg/L
K_R	—	Redlich–Peterson model isotherm constant, L/g
K_s	—	SIPS constant related to energy adsorption, L/mg
m	—	Mass of nDCPD, g
N	—	Number of data
n_s	—	SIPS model dimensionless parameter
q_{cal}	—	Calculated value of Cr(III) ions adsorbed in equilibrium, mg/g
q_d	—	Amount of chromium that remained adsorbed in nDCPD, mg/g
q_e	—	Concentration of Cr(III) in equilibrium with the solid phase, mg/g
q_{exp}	—	Experimental value of Cr(III) ions adsorbed in equilibrium, mg/g
q_m	—	Maximum Cr(III) concentration adsorbed by the adsorbent mass, mg/g
R	—	Ideal gases constant, kJ/mol K
R_L	—	Separation factor, dimensionless parameter
T	—	Absolute temperature, K
V	—	Solution volume, L
β	—	Redlich–Peterson model exponent $(0 < \beta < 1)$
ΔG	—	Gibbs free energy, kJ/mol
% Des	—	Cr(III) desorption percentage
% R_{Cr}	—	Cr(III) removal percentage
$1/n$	—	Adsorption reaction energy

Acknowledgments

The authors would like to thank the Mining, Metallurgy and Geology Engineering Department of Guanajuato University and UPIIG-IPN for the infrastructure provided to carry out this project. The authors also want to thank the Research and Postgraduate Secretariat for the financial support for this work (SIP: 20160593); other special thanks to the BIOCATEM Network, and finally the Cuero Centro, S.A. de C.V. company, for the donation of chromium salt.

References

[1] Ch.W. Cheung, Ch.K. Chan, J.F. Porter, G. McKay, Combined diffusion model for the sorption of cadmium, copper, and zinc ions onto bone char, Environ. Sci. Technol., 35 (2001) 1511–1522.
[2] T.G. Chuah, A. Jumasiah, I. Azni, S. Katayon, S.Y.T. Choong, Rice husk as a potentially low-cost biosorbent for heavy metal and dye removal: an overview, Desalination, 175 (2005) 305–316.
[3] K.K. Krishnani, X. Meng, C. Christodoulatos, V.M. Boddu, Biosorption mechanism of nine different heavy metals onto biomatrix from rice husk, J. Hazard. Mater., 153 (2008) 1222–1234.
[4] K. Pakshiranja, A.N. Worku, M.A. Acheampong, H.J. Lubberding, P.N.L. Lens, Cr(III) and Cr(VI) removal from aqueous solutions by cheaply available fruit waste and algal biomass, Appl. Biochem. Biotechnol., 170 (2013) 498–513.
[5] K.K. Singh, S.H. Hasan, M. Talat, V.K. Singh, S.K. Gangwar, Removal of Cr (VI) from aqueous solutions using wheat bran, Chem. Eng. J., 151 (2009) 113–121.
[6] U. Farroq, J.A. Kozinski, M.A. Khan, M. Athar, Biosorption of heavy metal ions wheat based biosorbents – a review on the recent literature, Bioresour. Technol., 101 (2010) 5043–5053.
[7] S. Rangabhashiyam, N. Selvaraju, B.R. Mohan, P.K.M. Anzil, K.D. Amith, E.R. Ushakumary, Hydrous cerium oxide nanoparticles impregnated *Enteromorpha* sp. for the removal of hexavalent chromium from aqueous solutions, J. Environ. Eng., 142 (2016) 1–9.
[8] J.V. Flores-Cano, A. Aragón-Pin, R. Leyva-Ramos, J.J. Salazar-Rabago, F. Carrasco-Marin, S. Leyva-Ramos, Adsorption mechanism of chromium(III) from water solution on bone char: effect of operating conditions, Adsorption, 22 (2016) 297–308.

[9] G. López-Téllez, C.E. Barrera-Díaz, P. Balderas-Hernández, G. Roa-Morales, B. Bilyeu, Removal of hexavalent chromium in aquatic solutions by iron nanoparticles embedded in orange peel pith, Chem. Eng. J., 173 (2011) 480–485.
[10] N.Ch. Feng, X. Guo, S. Liang, Y. Zhu, J. Liu, Biosorption of heavy metals from aqueous solutions by chemically modified orange peel, J. Hazard. Mater., 185 (2011) 49–54.
[11] E. Nakkeeran, S. Rangabhashiyam, M.S. Giri Nandagopal, N. Selvaraju, Removal of Cr (VI) from aqueous solution using *Strychnos nux-vomica* shell as an adsorbent, Desal. Wat. Treat., 57 (2016) 23951–2396.
[12] S. Rangabhashiyam, N. Selvaraju, Evaluation of the biosorption potential of a novel *Caryota urens* inflorescence waste biomass for the removal of hexavalent chromium from aqueous solutions, J. Taiwan Inst. Chem. Eng., 47 (2015) 59–70.
[13] S. Rangabhashiyam, M.S. Giri Nandagopal, E. Nakkeeran, N. Selvaraju, Adsorption of hexavalent chromium from synthetic and electroplating effluent on chemically modified *Swietenia mahagoni* shell in a packed bed column, Environ. Monit. Assess., 188 (2016) 411.
[14] S. Rangabhashiyam, M.S. Giri Nandagopal, E. Nakkeeran, R. Keerthi, N. Selvaraju, Use of Box–Behnken design of experiments for the adsorption of chromium using immobilized macroalgae, Desal. Wat. Treat., 57 (2016) 1–13.
[15] S. Rangabhashiyam, N. Selvaraju, Efficacy of unmodified and chemically modified *Swietenia mahagoni* shells for the removal of hexavalent chromium from simulated wastewater, J. Mol. Liq., 209 (2015) 487–497.
[16] E. Nakkeeran, N. Saranya, M.S. Giri Nandagopal, A. Santhiagu, N. Selvaraju, Hexavalent chromium removal from aqueous solutions by a novel powder, prepared from *Colocasia esculenta* leaves, Int. J. Phytorem., 18 (2016) 812–821.
[17] F. Fenglian, Q. Wang, Removal of heavy metal ions from wastewaters: a review, J. Environ. Manage., 92 (2011) 407–418.
[18] S. Gupta, B.V. Babu, Adsorption of Chromium (VI) by a Low-cost Adsorbent Prepared from Tamarind Seeds, Paper Presented at CHEMCON-2006, India, 27–30 Dec, 2006.
[19] S. Rangabhashiyam, E. Suganya, Alen Varghese Lity, Equilibrium and kinetics studies of hexavalent chromium biosorption on a novel green macroalgae *Enteromorpha* sp., Res. Chem. Intermed., 42 (2016) 1275–1294.
[20] M. Aliabadi, K. Morshedzadeh, H. Soheyli, Removal of hexavalent chromium from aqueous solution by lignocellulosic solid wastes, Int. J. Environ. Sci. Technol., 3 (2006) 321–325.
[21] S. Rangabhashiyam, E. Suganya, N. Selvaraju, Packed bed column investigation on hexavalent chromium adsorption using activated carbon prepared from *Swietenia mahagoni* fruit shells, Desal. Wat. Treat., 57 (2015) 13048–13055.
[22] W.S. Wan Ngah, M.A.K.M. Hanafiah, Removal of heavy metal ions from wastewater by chemically modified plant wastes as adsorbents: a review, Bioresour. Technol., 99 (2008) 3935–3948.
[23] H.A. Hegazi; Removal of heavy metals from wastewater using agricultural and industrial wastes as adsorbents, HBRC J., 9 (2013) 276–282.
[24] A. Fathima, R. Aravindhan, J. Raghava Rao, B. Unni Nair, Biomass of *Termitomyces clypeatus* for chromium(III) removal from chrome tanning wastewater, Clean Technol. Environ. Policy, 17 (2015) 541–547.
[25] G. Asgari, A.R. Rahmani, J. Faradmal, A. Motaleb, S. Mohammadi, Kinetic and isotherm of hexavalent chromium adsorption onto nano hydroxyapatite, J. Res. Health Sci., 12 (2012) 45–53.
[26] M. Sadat-Shojai, M.T. Khorasani, E. Dinpanah-Khoshdargi, A. Jamshidi, Synthesis methods for nanosized hydroxyapatite with diverse structures, Acta Biomater., 9 (2013) 7591–7621.
[27] J. Brzezińska-Miecznik, K. Haberko, M.M. Bućko, G. Grzegorz, M. Sitarz, Hydroxyapatite from animal bones – extraction and properties, Ceram. Int., 41 (2015) 4841–4846.
[28] T.A.R.M. Lima, N.S. Brito, J.A. Peixoto, M.E.G. Valerio, The incorporation of chromium (III) into hydroxyapatite crystals, Mater. Lett., 140 (2015) 187–191.
[29] S. Hokkanen, A. Bhatnagar, E. Repo, S. Lou, M. Sillanpää, Calcium hydroxyapatite microfibrillated cellulose composite as a potential adsorbent for the removal of Cr(VI) from aqueous solution, Chem. Eng. J., 283 (2016) 445–452.
[30] I. Mobasherpour, E. Salahi, M. Pazouki, Comparative of the removal of Pb^{2+}, Cd^{2+} and Ni^{2+} by nano crystallite hydroxyapatite from aqueous solutions: adsorption isotherm study, Arabian J. Chem., 5 (2012) 439–446.
[31] S.R. Dutta, D. Passi, P. Singh, A. Bhuibhar, Ceramic and non-ceramic hydroxyapatite as a bone graft material: a brief review, Irish J. Med. Sci., 184 (2015) 101–106.
[32] A. Doostmohammadi, A. Monshi, R. Salehi, M.H. Fathi, S. Karbasid, U. Pieles, A.U. Daniels, Preparation, chemistry and physical properties of bone-derived hydroxyapatite particles having a negative zeta potential, Mater. Chem. Phys., 132 (2012) 446–452.
[33] Ž. Radovanović, B. Jokić, D. Veljović, S. Dimitrijević, V. Kojić, R. Petrović, D. Janaćković, Antimicrobial activity and biocompatibility of Ag^{+}- and Cu^{2+}-doped biphasic hydroxyapatite/α-tricalcium phosphate obtained from hydrothermally synthesized Ag^{+} -and- Cu^{2+} doped hydroxyapatite, Appl. Surf. Sci., 307 (2014) 513–519.
[34] L. Hakim, Z. Yaakob, M. Ismail, W.R. Wan Daud, R. Sari, Hydrogen production by steam reforming of glycerol over Ni/Ce/Cu hydroxyapatite-supported catalysts, Chem. Pap., 67 (2013) 703–712.
[35] Y. Ono, T. Rachi, M. Yokouchi, Y. Kamimoto, A. Nakajima, K. Okada, Photo-oxidation of gaseous ethanol on photocatalyst prepared by acid leaching of Titanium oxide/hydroxyapatite composite, Mater. Res. Bull., 48 (2013) 2272–2278.
[36] H.R. Low, M. Avdeev, K. Ramesh, T.J. White, Zinc hydroxyapatite catalyst for decomposition of 2-propanol, Adv. Mater., 24 (2012) 4175–4179.
[37] C. Boucetta, M. Kacimi, A. Ensuque, J.Y. Piquemal, F. Bozon-Verduraz, M. Ziyad, Oxidative dehydrogenation of propane over chromium-loaded calcium-hydroxyapatite, Appl. Catal., A, 356 (2009) 201–210.
[38] A.L. Giraldo-Betancur, D.G. Espinosa-Arbelaez, A. del Real-López, B.M. Millan-Malo, E.M. Rivera-Muñoz, E. Gutierrez-Cortez, P. Pineda-Gomez, S. Jimenez-Sandoval, M.E. Rodriguez-García, Comparison of physicochemical properties of bio and commercial hydroxyapatite, Curr. Appl. Phys., 13 (2013) 1383–1390.
[39] T. Wen-Qing, Z. Rong-Ying, F. Yong-Lan, L. Xiao-Ming, Z. Wei, Removal of Cr(VI) from aqueous solution by nano-carbonate hydroxylapatite of different Ca/P molar ratios, Chem. Eng. J., 223 (2013) 340–346.
[40] F. Fernane, S. Boudia, F. Aiouache, Removal Cu (II) and Ni (II) by natural and synthetic hydroxyapatites: a comparative study, Desal. Wat. Treat., 52 (2014) 2856–2862.
[41] Y. Huang, L. Chen, H. Wang, Removal of Co (II) from aqueous solution by using hydroxyapatite, J. Radioanal. Nucl. Chem., 291 (2012) 777–785.
[42] M. Kapur, M.K. Mondal, Competitive sorption of Cu (II) and Ni (II) ions from aqueous solutions: kinetics, thermodynamics and desorption studies, J. Taiwan Inst. Chem. Eng., 45 (2014) 1803–1813.
[43] F. Tamimi, S. Zeeshan, J. Barralet, Dicalcium phosphate cements: brushite and monetite, Acta Biomater., 8 (2012) 474–487.
[44] D. Pham Minh, N.D. Tran, A. Nzihou, P. Sharrock, Calcium phosphate based materials starting from calcium carbonate and orthophosphoric acid for the removal of lead (II) from an aqueous solution, Chem. Eng. J., 243 (2014) 280–288.
[45] M. Mourabet, H. El Boujaady, A. El Rhilassi, H. Ramdane, M. Bennani-Ziatni, R. El Hamri, A. Taitai, Defluoridation of water using brushite: equilibrium, kinetic and thermodynamic studies, Desalination, 278 (2011) 1–9.
[46] H.E.L. Madsen, Influence of foreign metal ions on crystal growth and morphology of brushite ($CaHPO_4{\cdot}2H_2O$) and its transformation to octacalcium phosphate and apatite, J. Cryst. Growth, 310 (2008) 2602–2612.
[47] A. El Hamidi, S. Arsalane, M. Malim, Kinetics and isotherm studies of copper removal by brushite calcium phosphate: linear and non-linear regression comparison, E-J. Chem., 9 (2012) 1532–1542.

[48] A. El Hamidi, R. Mulongo Masamba, M. Khachani, M. Halim, S. Arsalane, Kinetics modeling in liquid phase sorption of copper ions on brushite di-calcium phosphate di-hydrate $CaHPO_4{\cdot}2H_2O$ (DCPD), Desal. Wat. Treat., 56 (2015) 779–791.
[49] I.G. Becerril-Juárez, R.A. Morales-Luckie, F. Ureña-Nuñez, J.A. Arenas-Alatorre, J.P. Hinestroza, V. Sanchez-Mendieta, Silver micro-, submicro- and nano-crystals using bovine bone as template. Formation of a silver/bovine bone composite, Mater. Lett., 85 (2012) 157–160.
[50] D.L. Trimm, Thermal Stability of Catalyst Support, C.H. Bartholomew, J.B. Butt, Eds., Catalyst Deactivation, Elsevier Science, Vol. 68, United States, 1991.
[51] J.P. Reymond, F. Kolenda, Estimation of the point of zero charge of simple and mixed oxides by mass titration, Powder Technol., 103 (1999) 30–36.
[52] G. Blázquez, M. Calero, A. Ronda, G. Tenorio, M.A. Martín-Lara, Study of kinetics in the biosorption of lead onto native and chemically treated olive stone, J. Ind. Eng. Chem., 20 (2014) 2754–2760.
[53] R. Sudha, K. Srinivasan, P. Premkumar, Removal of nickel (II) from aqueous solution using *Citrus limettioides* peel and seed carbón, Ecotoxicol. Environ. Saf., 117 (2015) 115–123.
[54] X.S. Wang, Y. Zhou, Y. Jiang, C. Sun, The removal of basic dyes from aqueous solutions using agricultural by-products, J. Hazard. Mater., 157 (2008) 374–385.
[55] S. Elabbas, L. Mandi, F. Berrekhis, M.N. Pons, J.P. Leclerc, N. Ouazzani, Removal of Cr (III) from chrome tanning wastewater by adsorption using two natural carbonaceous materials: eggshell and powdered marble, J. Environ. Manage., 166 (2016) 589–595.
[56] N. Saranya, E. Nakkeeran, S. Shrihari, N. Selvaraju, Equilibrium and kinetic studies of hexavalent chromium removal using a novel biosorbent: *Ruellia patula* Jacq, Arab. J. Sci. Eng., 42 (2017) 1545–1557.
[57] E. Suganya, S. Rangabhashiyam, A.V. Lity, N. Selvaraju, Removal of hexavalent chromium from aqueous solution by a novel biosorbent *Caryota urens* seeds: equilibrium and kinetic studies, Desal. Wat. Treat., 57 (2016) 23940–23950.
[58] N. Saranya, E. Nakeeran, M.S. Giri Nandagopal, N. Selvaraju, Optimization of adsorption process parameters by response surface methodology for hexavalent chromium removal from aqueous solutions using *Annona reticulata* Linn peel microparticles, Water Sci. Technol., 75 (2017) 2094–2107.
[59] K. Pei-Sin, H. Yung-Tse, L. Siew-Ling, O. Siew-Teng, H. Sie-Tiong, Removal of hazardous heavy metals from aqueous environment by low-cost adsorption materials, Environ. Chem. Lett., 12 (2014) 15–25.
[60] E. Pehlivan, E. Pehlivan, H. Tutar Kahraman, Hexavalent chromium removal by Osage Orange, Food Chem., 133 (2012) 1478–1484.
[61] R. Vani, E.K. Girija, M. Palanichamy, S. Narayana Kalkura, Simultaneous crystallization of calcium phosphate and calcium oxalate in the presence of ascorbic acid under physiological conditions, Mater. Sci. Eng., C, 29 (2009) 1227–1232.
[62] M. Parvinzadeh Gashti, M. Bourquin, M. Stir, J. Hulliger, Glutamic acid inducing kidney stone biomimicry by a brushite/gelatin composite, J. Mater. Chem. B, 1 (2013) 1501–1508.
[63] V. Thangadurai, P. Kopp, Chemical synthesis of Ca-doped CeO_2—intermediate temperature oxide ion electrolytes, J. Power Sources, 168 (2007) 178–183.
[64] M. Suat Aksoy, Study of the interaction between chromium (III) and hydroxamic acids, J. Chem. Eng. Data, 55 (2010) 2252–2256.
[65] T. Sopcak, L. Medvecky, M. Giretova, R. Stulajterova, J. Durisin, V. Girman, M. Faberova, Effect of phase composition of calcium silicate phosphate component on properties of brushite based composite cements, Mater. Charact., 117 (2016) 17–29.
[66] S.M. Arifuzzaman, S. Rohani, Experimental study of brushite precipitation, J. Cryst. Growth, 267 (2004): 624–634.
[67] B.M. Weckhuysen, A.A. Verberckmoes, J. Debaere, K. Ooms, I. Langhans, R.A. Schoonheydt, In situ UV–Vis diffuse reflectance spectroscopy – on line activity measurements of supported chromium oxide catalysts: relating isobutane dehydrogenation activity with Cr-speciation via experimental design, J. Mol. Catal. A: Chem., 151 (2000) 115–131.
[68] M.M. Mirković, T.D. Lazarević Pašti, A.M. Došen, M.Ž. Čebela, A.A. Rosić, B.Z. Matović, B.M. Babić, Adsorption of malathion on mesoporous monetite obtained by mechanochemical treatment of brushite, RSC Adv., 6 (2016) 12219–12225.